Nuclear Instruments and Methods in Physics Research A 836 (2016) 1–6

Contents lists available at ScienceDirect

Nuclear Instruments and Methods in Physics Research A

journal homepage: www.elsevier.com/locate/nima

CsI–Silicon Particle detector for Heavy ions Orbiting in Storage rings (CsISiPHOS)

M.A. Najafi [a,b,c,*], I. Dillmann [a,c,d], F. Bosch [a], T. Faestermann [b], B. Gao [a,e,f], R. Gernhäuser [b], C. Kozhuharov [a], S.A. Litvinov [a], Yu.A. Litvinov [a], L. Maier [b], F. Nolden [a], U. Popp [a], M.S. Sanjari [a], U. Spillmann [a], M. Steck [a], T. Stöhlker [a], H. Weick [a]

[a] GSI Helmholtzzentrum für Schwerionenforschung, Darmstadt, Germany
[b] Technische Universität München, Germany
[c] Justus-Liebig Universtät Giessen, Germany
[d] TRIUMF, Vancouver, Canada
[e] Max Planck Institut für Kernphysik, Heidelberg, Germany
[f] Institute of Modern Physics, Chinese Academy of Sciences, China

ARTICLE INFO

Article history:
Received 8 October 2015
Received in revised form
18 August 2016
Accepted 20 August 2016
Available online 22 August 2016

Keywords:
Heavy-ion detectors
Silicon sensors
CsI(Tl) scintillators
Particle identification
Decay spectroscopy

ABSTRACT

A heavy-ion detector was developed for decay studies in the Experimental Storage Ring (ESR) at the GSI Helmholtz Centre for Heavy Ion Research in Darmstadt, Germany. This detector serves as a prototype for the in-pocket particle detectors for future experiments with the Collector Ring (CR) at FAIR (Facility for Antiproton and Ion Research). The detector includes a stack of six silicon pad sensors, a double-sided silicon strip detector (DSSD), and a CsI(Tl) scintillation detector. It was used successfully in a recent experiment for the detection of the β^+-decay of highly charged $^{142}Pm^{60+}$ ions. Based on the $\Delta E/E$ technique for particle identification and an energy resolution of 0.9% for ΔE and 0.5% for E (Full Width at Half Maximum (FWHM)), the detector is well-suited to distinguish neighbouring isobars in the region of interest.

1. Introduction

The β-decay experiments of highly charged ions at the experimental storage ring (ESR) at GSI Darmstadt have been a rich source of new discoveries about decay properties of nuclei [1,2]. The exciting discovery of the bound-state β^- decay in 1992 [3,4], the discovery of new isotopes and accurate measurements of their masses with Schottky and isochronous mass spectrometry [5,6], and finding new long-lived K-isomers [7,8] are a few examples of the accomplishments from the FRS-ESR facility. In the ESR, ion beams of different charge state can be cooled down to a relative momentum spread of $\Delta p/p = 3 \times 10^{-5}$, and be stored for up to a few hours. In order to achieve such performance, the ESR is kept at ultra-high vacuum (UHV) conditions of around 10^{-11} mbar, which is very difficult to reach with detectors inside the UHV area of the storage ring [9]. Therefore, except in very special cases, the particle detectors of the ESR are placed inside so-called pockets, which are small rectangular stainless steel tubes with a cross section of 37×57 mm^2. The vacuum of the ring is then separated from the air pressure inside the pocket by a window on the pocket that is usually made of a 25 μm stainless-steel foil. More information about the ESR detector pockets and their positions in the ring can be found in Reference [10].

In this paper we report the design and first results of a new multi-purpose detector developed for storage ring experiments, CsISiPHOS (CsI–Silicon Particle detector for Heavy ions Orbiting in Storage rings). The detector is a prototype for the particle detectors for the ILIMA programme (Isomers, LIfetimes, and MAsses) [11] in the future Collector Ring (CR), planned at the Facility for Antiproton and Ion Research, FAIR [12]. In addition, it was foreseen to be used in two ESR experiments: the bound-state β-decay of ^{205}Tl, and the β^+-decay rate of $^{142}Pm^{60+}$. The data presented in this report are from the second experiment.

2. Detector design

The configuration of the sensors was partially motivated by the previous version of the in-pocket particle detectors [13], developed about 10 years ago by Ludwig Maier for the measurement of the bound-state β decay rate of fully ionised ^{207}Tl in the ESR (see

* Corresponding author. Current address: KVI-CART, University of Groningen, The Netherlands.
E-mail address: m.a.najafi@gsi.de (M.A. Najafi).

http://dx.doi.org/10.1016/j.nima.2016.08.040
0168-9002/

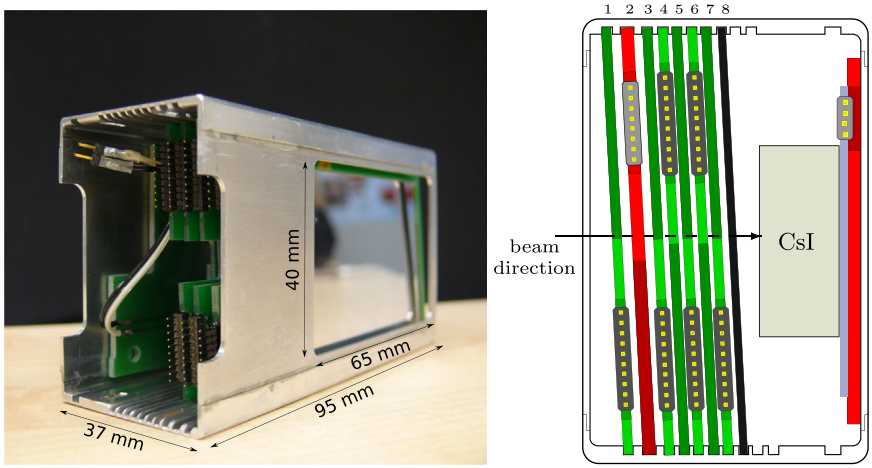

Fig. 1. *Left*: Photo of the fully equipped detector. The entrance window has the dimensions 65×40 mm^2. *Right*: Schematic drawing of CsISiPHOS showing the arrangement of the subdevices. The silicon sensors were tilted by 3° to reduce the channelling effect. The configuration of the sensors from left to right is given in the text.

Table 1
Comparison of Maier's particle detector with CsISiPHOS.

Detector specification	Maier's detector	CsISiPHOS
ΔE measurement	14 Si PIN diodes (400 μm)	6 Si pad sensors
Position measurement	2 SSSDs	1 DSSD
Residual energy	No	CsI(Tl) scintillator
# readout channels	22	54
Active area	18×20 mm^2	40×60 mm^2

Figure 22 in Reference [1]). The new detector is constructed based on an improved design, namely, the active area has been increased by a factor of 6, and its modular design can flexibly be adjusted for different experimental requirements. (see Fig. 1). Moreover, a CsI (Tl) scintillation detector was added in the new design as a beam stopper for total energy reconstruction. The CsI(Tl) crystal is coupled to a silicon photodiode (on the p side), mounted on a circuit board, which is glued to the end wall of a dedicated frame. Table 1 gives a list of properties of the current design (CsISiPHOS) and of its precursor for comparison.

The frame has 10 positions that can be filled with silicon sensors or passive degraders of suitable thickness. The configuration of the positions for this experiment was as follows (the parenthesis indicates the silicon surface that faces the beam):

- Position 1: silicon pad sensor (n side)
- Position 2: double-sided silicon strip detector, DSSD (p side)
- Positions 3–7: silicon pad sensors (n/p/n/p/n sides, respectively)
- Position 8: passive degrader, tantalum in the present work
- Positions 9 and 10: empty

For the most compact design, maximum flexibility, and a single PCB layout for the silicon pad sensors, consecutive layers are mounted in alternating orientation. As additional advantages the sensor sides facing each other are supplied with similar electric potential and thus avoid problems with leakage current or sparks in such a compact setup. Also a much more relaxed connector arrangement can be used with this solution. The passive degrader is a 1000 ± 8 μm thick slab of tantalum. All silicon sensors were tilted by an angle of 3° with respect to the entrance window of the frame. This tilting reduces the influence of the silicon crystal orientation on the pulse shape of the ions, the so-called "channelling effect" [14].

For the current version of CsISiPHOS, we have used a set of three different sensor types. The silicon pad sensors are based on the Design I chip by Micron semiconductor Ltd, England, and the photodiode is a MSD35 chip from the same manufacturer. The design I is a single-sided silicon strip detector (SSSD), which is operated as a pad sensor in our setup, and its metalisation is a layer of aluminium with a thickness of 0.5 μm. The p side metalisation of the photodiode has a grid structure (9G) with a thickness of 0.05 μm covering less than 2% of the active area. The DSSD was manufactured by Canberra Inc, USA (PF-60CT-40CD-60∗40-300). More information about these chips is given in Table 2. The CsI(Tl) crystal has a thickness of 10 mm and an area of 24×24 mm^2, not wide enough to cover the active area of the detector. The CsI(Tl) crystal was coupled to the silicon photodiode using optical cement (BC-600 by Saint Gobain Crystals, France), and then wrapped in highly specular reflective foil (Vikuiti Projection Film manufactured by 3M, USA) to optimise homogeneous light collection. The foil includes a layer of Acrylate adhesive laminated onto a layer of PVC, giving a total thickness of 0.3 mm.

The fully equipped detector (Fig. 1, left) was read out through 54 channels: 8×6 channels for the silicon pad detectors, 4 channels for the DSSD, and 2 channels for the CsI(Tl). The DSSD has 100 strips, and the strips of each side are connected to a chain of resistors with a total resistance of 3000 Ω (60 resistors of 50 Ω on the p side, and 40 resistors of 75 Ω on the n side). The position of the incident particles is obtained by the difference of the signal height at the two ends of each resistor chain. The signals were transferred from the detector units to the flange of the pocket using two 50 Ω flat cables from Samtec Inc., USA. Each cable consists of 60 individually shielded wires, and is coupled to connectors on both ends with a pin pitch of 0.5 mm. The shields are connected to the ground on one end.

The analogue signals from the detector were extracted using charge-sensitive preamplifiers MPR-32 and MSI-8 (Mesytec, Germany). The p side strips of the silicon pad detectors (6×7

Table 2
Properties of the silicon sensors. The silicon pad sensors are based on Design I-500 chip by Micron semiconductor Ltd, England, and the photodiode is a MSD35 chip of the same manufacturer. The Design I chip is commonly used as a single-sided silicon strip detector (SSSD), but in this work, it was operated as a pad sensor. The DSSD was manufactured by Canberra Inc, USA (PF-60CT-40CD-60∗40-300). The thicknesses are given perpendicular to the surface of the detector, and the 3° tilting adds 0.1% to the thickness along the beam direction.

Si sensors	Active area	Thickness (μm)	p side	n side
Pad sensor	60 mm × 40 mm	500	7 strips	No segmentation
DSSD	60 mm × 40 mm	300	60 strips	40 strips
Photodiode	⌀35 mm	1000	Grid	No segmentation

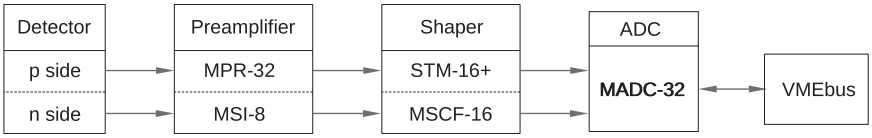

Fig. 2. The electronics readout of the experiment. For the DSSD and the silicon photodiode, both sides were connected to the MSI-8 preamplifier. Both sides of each silicon detector were connected to a preamplifier.

channels) were connected to two MPR-32 modules, because their output signals have the same shape and amplitude. MPR-32 processes all input channels with the same polarity and an identical amplification factor. The other channels, including the n side of the silicon pad detectors, both sides of the DSSD, and the photodiode were connected to two MSI-8 modules. MSI-8 is a flexible preamplifier box with the possibility of reading signals with different amplitudes on different channels, and also applying different voltages to different detector channels. Although the MSI-8 modules include shapers, only the preamplifier part was used. The MSCF-16 and STM-16 shapers (Mesytec, Germany) were used to shape (with a shaping time of 2 μs) and further amplify the signals. The shaped signals were digitised with MADC-32 analogue to digital converters and transferred to the storage disk via a VMEbus (Versa Module Europa bus) (see Fig. 2) operated by the data acquisition software MBS, developed at GSI [15].

3. Experiment at the ESR

A primary beam of ^{152}Sm was accelerated up to an energy of 550 MeV/u by the Schwerionen Synchrotron (SIS18) at GSI Darmstadt, and impinged on a 2.5 g/cm^2 thick beryllium target at the entrance of the fragment separator (FRS) to produce secondary ions of interest. The H-like ^{142}Pm^{60+} ions were separated using the FRS [16], and then injected into the ESR to be cooled and stored for decay measurements. The preparation of the beam prior to injection in the ESR was the same as in Reference [17]. The primary physics goal of the experiment was to extend the study of the recently observed modulations in the electron-capture decay rate of H-like ^{142}Pm^{60+} and ^{140}Pr^{58+} [18]. A few hours of the beam time were assigned to the commissioning of CsISiPHOS by measurements of the β^+-decay of ^{142}Pm^{60+}. It was placed behind the first dipole after a straight section, outside of the stable trajectory.

Neutral ^{142}Pm atoms (Z=61) decay with a branching ratio of 96.4% to the ground state of the stable ^{142}Nd (Z=60), while the remaining 3.6% of the decays end up in excited states [19] (see Fig. 3). Therefore, in almost all of the decays in this experiment the decay products are in the ground state. CsISiPHOS was placed so that it only observes the β^+-decay products (^{142}Nd^{59+}) and the parent ions that pick up an electron in their atomic shells within the electron cooler or in the residual gas of the ESR (^{142}Pm^{59+}). Assuming a known loss rate of the stored ^{142}Pm^{60+} ions due to atomic processes, the time-dependent rate of daughter ions detected may be used as a direct measure of its total decay constant for β^+/EC decay.

During the commissioning of CsISiPHOS, a few tens of measurement cycles were performed. Fig. 4 shows an example for one measurement cycle. In each cycle, a few hundred ^{142}Pm^{60+} ions were injected into the ring, and after 3 s stochastic cooling they were cooled further using the electron cooler. About 6 s after the injection, the detector pocket was moved towards the fully cooled beam until the front edge of the detector is 22 mm from the centre of the beam pipe (a displacement of 89 mm done within about 0.25 s). At this position, the shifted trajectories of the β^+-decay daughter ions, ^{142}Nd^{59+}, hit the detector behind the vacuum window. A measurement period of 4 min was applied, during which most of the mother ions decay ($t_{1/2}$ = 39.2 ± 0.7 s [20]). A signal by any of the silicon pad sensors triggered the data acquisition system to record the event. At the end of each cycle (246 s after the injection) the ring was cleared of any remaining ions using a scraper, to prepare for the next cycle.

4. Analysis and results

The calibration of the energy spectra is based on the calculation of the energy-loss of heavy ions penetrating matter using the ATIMA code [21]. Thanks to the use of an electron cooler, the cooled ion beams in the ESR have a very low momentum spread $\Delta p/p$ and thus a well-defined kinetic energy, in our case 400 MeV/u. Using this value, the calculated energy-loss values were applied to the ADC values read out from the detector channels. The ADC offsets were taken into account using data from a pulse generator with four different pulse amplitudes.

After calibration of all channels, the energy signals of the silicon pad sensors (E_i) were summed event-by-event to obtain $\Delta E = \sum_i E_i$. The use of the resistor chains for the readout of the DSSD increases the uncertainties of its energy signals. Therefore, the DSSD was excluded from the sum to improve the ΔE resolution. The energy loss histogram, shown in the left panel of Fig. 5 in black, has two peaks which can be identified as H-like ^{142}Nd^{59+} from the β^+-decay of H-like ^{142}Pm^{60+} and the atomic electron recombination of bare ^{142}Nd^{60+}, and He-like ^{142}Pm^{59+} from the atomic electron recombination of H-like ^{142}Pm^{60+}. Another possibility, which can happen only in the detector itself, is the

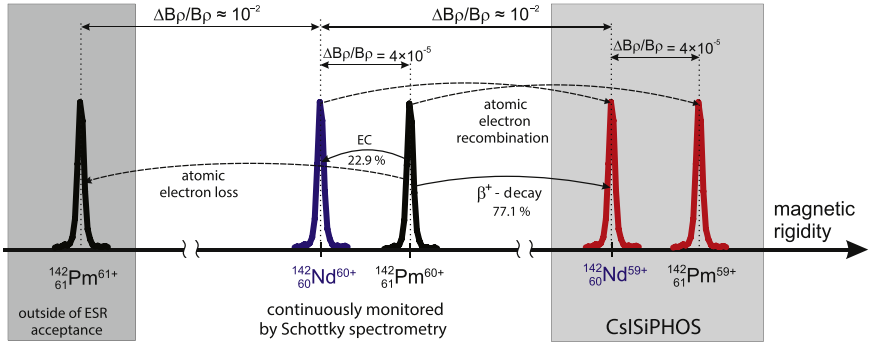

Fig. 3. Possible decay channels in the experiment. Nuclear and atomic interactions are shown with solid and dashed lines, respectively.

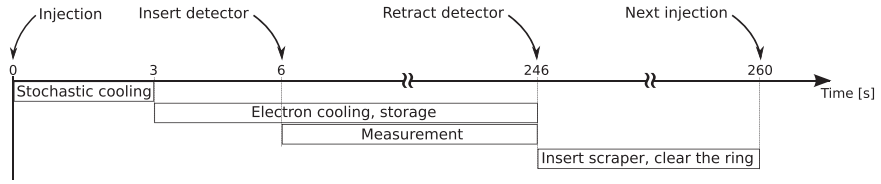

Fig. 4. Measurement cycle.

creation of $^{142}Nd^{59+}$ by orbital electron capture of $^{142}Pm^{59+}$ (see Fig. 3).

Since the energy loss of ions with the same velocity scales with the square of the atomic number, Z^2, the peak at higher energies can only be from the recombined parent ion, $^{142}Pm^{59+}$. The blue histogram in the right panel of Fig. 5 shows the events with a condition on the energy loss, namely $\Delta E > 6.8$ MeV. It appears that the $^{142}Pm^{59+}$ ions hit two different positions on the DSSD, depending on the position of electron recombination.

The position of the pocket was adjusted so that the β^+-decay daughter ions, $^{142}Nd^{59+}$, hit CsISiPHOS roughly at the centre of the sensitive area. Looking in the direction of the beam momentum, this adjustment puts the centre of the DSSD at 52 mm outside of the central axis of the ESR beam pipe. CsISiPHOS detects $^{142}Nd^{59+}$ and $^{142}Pm^{59+}$ ions at distances of approximately 54 mm and 73 mm from the centre of the beam pipe, respectively.

The measured energies in the CsI(Tl) scintillator are also used for particle identification. Fig. 6 shows the energy spectrum of the CsI(Tl) scintillator, with a main peak at 37.5 GeV which is from $^{142}Nd^{59+}$ ions, and a smaller peak at lower energies of 36.6 GeV, which is from the recombined parent ions, $^{142}Pm^{59+}$. The trajectory of the $^{142}Pm^{59+}$ ions do not hit the CsI(Tl) scintillator under normal circumstances since the crystal is smaller than the Si pad sensors and the DSSD. However, if the $^{142}Pm^{60+}$ ions capture an electron in the last magnet it is possible for some of the $^{142}Pm^{59+}$ ions to hit the scintillator. The histogram of the energy loss in the silicon pad sensors, ΔE, versus the energy of CsI(Tl), E_{CsI}, is shown in Fig. 7, in which these two groups of events are indicated by blue circles and can be clearly distinguished.

In addition, there are two groups of events shown with red circles. These events might have been produced via the stochastic cooling, which has a limited acceptance for the revolution frequencies. If the revolution frequency is outside the acceptance, the stochastic cooling causes the ions to heat up. The heated ions can be stored in the ring for a short time, and eventually recombine with electrons through collisions with the rest gas or in the electron cooler and thus hit the detector.

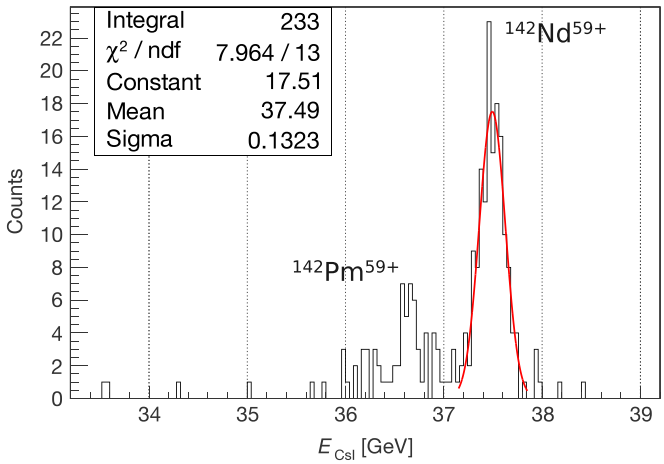

Fig. 6. Energy spectrum of the CsI(Tl) scintillator. The red curve is a Gaussian function fitted to the histogram. (For interpretation of the references to color in this figure caption, the reader is referred to the web version of this paper.)

Fig. 8 shows the total energy spectrum, obtained by summing the energy loss of the beam in all components of CsISiPHOS, event by event: $E_{total} = \Delta E + E_{DSSD} + E_{Ta} + E_{CsI}$. To avoid systematic uncertainties the energy loss of the particles in the tantalum degrader, E_{Ta}, was extrapolated from the measured energy loss in the silicon pad detectors, ΔE, by a constant scaling factor R, for each element. From a detailed ATIMA calculation, the average energy loss of $^{142}Nd^{59+}$ in six layers of silicon pad detectors was determined to derive R as the ratio of the energy loss in Ta from ATIMA (E_{Ta}^{ATIMA}) and the sum of energy losses in the silicon pad detectors from ATIMA (ΔE^{ATIMA}),

$$R = \frac{E_{Ta}^{ATIMA}}{\Delta E^{ATIMA}}.$$

Then we calculate $E_{Ta} = R \cdot \Delta E$ per event.

The energy resolution values for CsISiPHOS have been

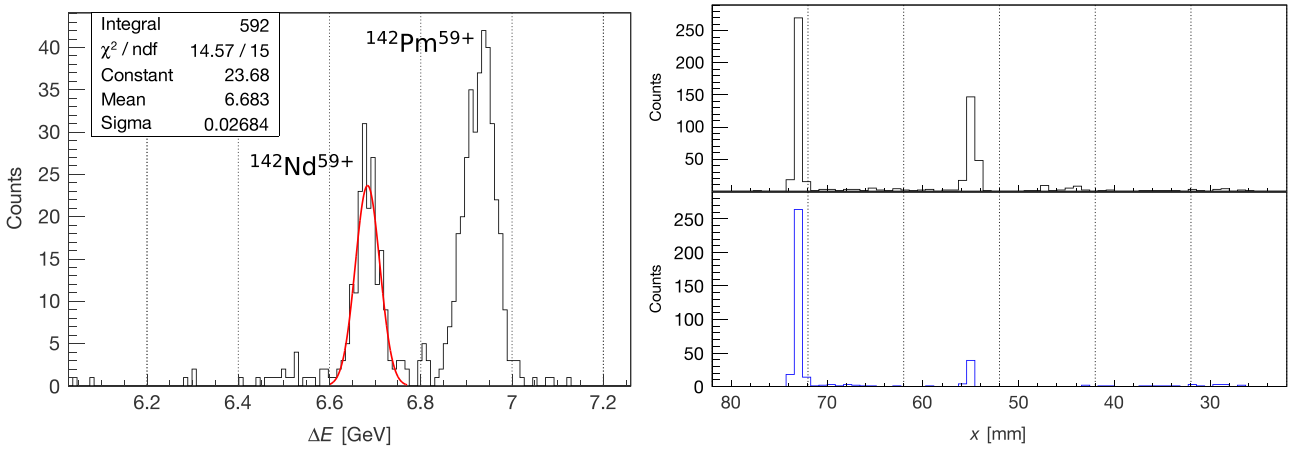

Fig. 5. *Left*: Energy loss spectrum of the silicon pad sensors, $\Delta E = \sum_i E_i$. The red curve is a Gaussian function fitted to the histogram. *Right*: Position histogram of the ions on the DSSD, with origin on the central axis of the ESR beam pipe. The blue histogram represents the events with a condition on the energy loss, namely $\Delta E > 6.8$ MeV. (For interpretation of the references to color in this figure caption, the reader is referred to the web version of this paper.)

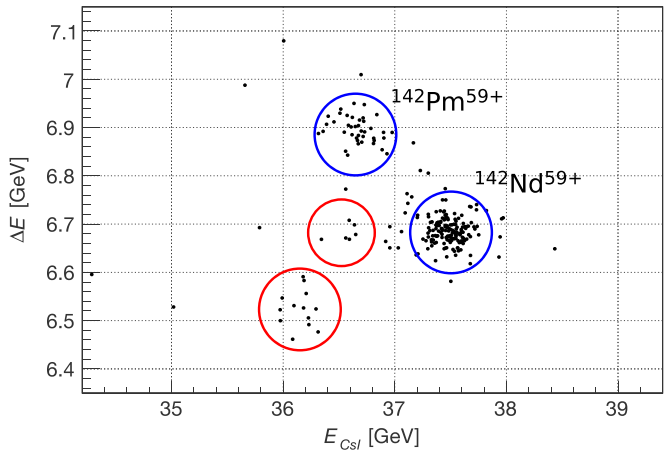

Fig. 7. Energy loss in silicon pad sensors, ΔE, versus CsI(Tl) energy, E_{CsI}. The red circles show a few unexpected events whose origin is still unknown (see text for more explanation). (For interpretation of the references to color in this figure caption, the reader is referred to the web version of this paper.)

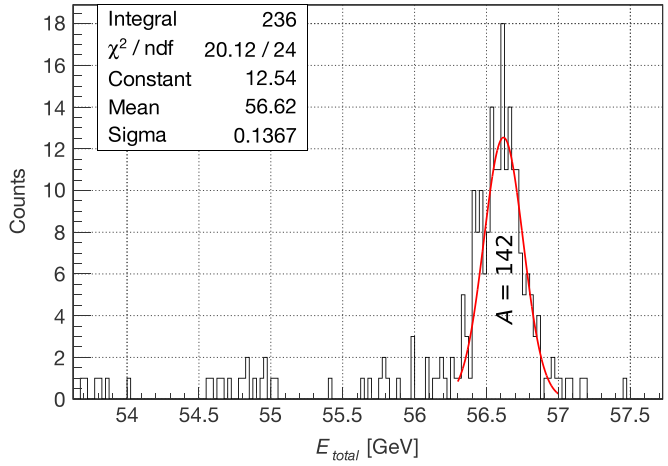

Fig. 8. Total energy reconstruction, $E_{total} = \Delta E + E_{DSSD} + E_{Ta} + E_{CsI}$. The energy loss in the entrance foil of the pocket is around 160 MeV, which is not added to this sum.

determined by fitting Gaussian distributions to the spectra, giving:

FWHM(ΔE): 60 MeV at 6. 7 GeV

FWHM(E_{CsI}): 0. 3 GeV at 37. 5 GeV

FWHM(E_{total}): 0. 3 GeV at 57. 0 GeV

With this resolution the neighbouring ions in the range of interest are well distinguished. The electronic noise of each silicon pad detector is around 3 MeV FWHM, and the combination of the CsI (Tl) and the silicon photodiode has an electronic noise of around 30 MeV FWHM. The energy loss variations due to the distribution of incidence angles are negligible, because the incidence angle of the decay ions is smaller than 0.17°.

The ATIMA calculations give an energy straggling of around 33 MeV in the Ta absorber, and since E_{Ta} was determined by scaling ΔE, the uncertainties from ΔE are multiplied by a factor of 1.8. Nevertheless, the straggling in the Ta absorber remains a small contribution to the total energy resolution of 300 MeV FWHM. This indicates that probably the energy resolution in the CsI(Tl) detector is the limiting factor. Due to the compact geometry and the difficult wrapping of a rectangular scintillator on a round shaped silicon photodiode, it is likely that the light collection was not homogeneous.

The observed ΔE resolution $d(\Delta E)/\Delta E = 0.9\%$ corresponds to a Z resolution of $dZ/Z = 0.45\%$ or $dZ=0.27$ (FWHM) for separation of elements around $Z=61$. If scaled linearly to $Z=81$ the resolution for separation of elements is expected to be around $dZ = 0.27 \times (61/81) = 0.20$, about 36% of the resolution obtained in the work of Maier, $dZ=0.55$ (FWHM) [13].

CsISiPHOS can stop Tl and heavier ions at 400 MeV/u without a passive absorber, and the Ta absorber can be replaced by a silicon pad detector in such experiments. Therefore, for the future measurement of the bound-state β-decay rate of ^{205}Tl a better performance is expected.

5. Conclusion and outlook

A new particle detector, CsISiPHOS, has been developed and successfully commissioned in a recent experiment at the ESR at GSI Darmstadt. The detector serves as a $\Delta E/E$ telescope for the detection and identification of heavy ions. In addition, the position of incident ions is determined using a DSSD, which can be used to determine the trajectories of the decay products at the detector position. In some cases, the parent ions that pick up an electron in their atomic shells during their up to 40 million kilometres (on average) long flight path through the ESR can also be detected. The measured spectra can be used in future dedicated experiments to benchmark ion-optical calculations of the ESR storage ring.

This detector is also a prototype of particle detectors for future storage ring experiments. In order to improve the employed detection technique detector pockets with a larger space along the beam direction can be used. In that case more silicon sensors or a thicker CsI(Tl) scintillator can be used to stop the ions. Such improvements have already been taken into account in the design of the future Collector Ring (CR) at FAIR.

Acknowledgment

The authors gratefully acknowledge the contributions of the technical support team of the ESR and the GSI accelerator operators. We appreciate the help of M. Böhmer from the electronics division of TU München for his insightful improvements to our circuit boards, R. Lang and M. Klöckner from the mechanical workshop of TU München, and B. Kindler and B. Lommel from the target lab of GSI. This work has been funded via the BMBF projects 05P12RGFNJ (Multi-purpose pocket detector for in-ring decay spectroscopy) and 05P15WOFNA, the Helmholtz-CAS Joint Research Group HCJRG-108, the joint Max Planck/CAS doctoral promotion programme, partially by the Helmholtz association via the Young Investigators Project LISA; Lifetime Spectroscopy for Astrophysics (VH NG 627), and the Maier-Leibnitz Laboratory in Munich, and also supported by the DFG cluster of excellence "Origin and Structure of the Universe".

References

[1] Y.A. Litvinov, F. Bosch, Beta decay of highly charged ions, Rep. Prog. Phys. 74 (1) (2011) 016301.
[2] F. Bosch, Y.A. Litvinov, T. Stöhlker, Nuclear physics with unstable ions at storage rings, Prog. Part. Nucl. Phys. 73 (2013) 84–140.
[3] M. Jung, et al., First observation of bound-state β^- decay, Phys. Rev. Lett. 69 (1992) 2164–2167.
[4] F. Bosch, et al., Observation of bound-state β^- decay of fully ionized ^{187}Re: ^{187}Re-^{187}Os cosmochronometry, Phys. Rev. Lett. 77 (1996) 5190–5193.
[5] L. Chen, et al., Discovery and investigation of heavy neutron-rich isotopes with time-resolved Schottky spectrometry in the element range from thallium to actinium, Phys. Lett. B 691 (5) (2010) 234–237.
[6] D. Shubina, et al., Schottky mass measurements of heavy neutron-rich nuclides in the element range $70 \le Z \le 79$ at the GSI experimental storage ring,

Phys. Rev. C 88 (2013) 024310.
[7] G.D. Dracoulis, Isomers, nuclear structure and spectroscopy, Phys. Scr. 2013 (T152) (2013) 014015.
[8] M.W. Reed, et al., Discovery of highly excited long-lived isomers in neutron-rich hafnium and tantalum isotopes through direct mass measurements, Phys. Rev. Lett. 105 (2010) 172501.
[9] O. Klepper, et al., First steps towards radioactive beams in the Experimental Storage Ring at GSI, Nucl. Instrum. Methods B 70 (1–4) (1992) 427–433.
[10] O. Klepper, C. Kozhuharov, Particle detectors for beam diagnosis and for experiments with stable and radioactive ions in the storage-cooler ring ESR, Nucl. Instrum. Methods B 204 (2003) 553–556.
[11] P. Walker, Y.A. Litvinov, H. Geissel, The ILIMA project at FAIR, Int. J Mass Spectrom. 349–350 (2013) 247–254.
[12] A. Dolinskii, et al., The CR storage ring in an isochronous mode operation with nonlinear optics characteristics, Nucl. Instrum. Methods B 266 (19–20) (2008) 4579–4582.
[13] L.W. Maier, Speicherringexperiment zum gebundenen Beta-Zerfall vollstaendig ionisierter ^{207}Tl Kerne (Ph.D. thesis), Technische Universität München, Germany, 2007.
[14] L. Bardelli, et al., Influence of crystal-orientation effects on pulse-shape-based identification of heavy-ions stopped in silicon detectors, Nucl. Instrum. Methods A 605 (3) (2009) 353–358.
[15] N. Kurz, MBS Website. ⟨https://www.gsi.de/work/fairgsi/rare_isotope_beams/electronics/datenverarbeitung/datenerfassung/mbs.htm⟩, 1992.
[16] H. Geissel, et al., The GSI projectile fragment separator (FRS); a versatile magnetic system for relativistic heavy ions, Nucl. Instrum. Methods B 70 (1992) 286–297.
[17] P. Kienle, et al., High-resolution measurement of the time-modulated orbital electron capture and of the decay of hydrogen-like ^{142}Pm^{60+} ions, Phys. Lett. B 726 (4–5) (2013) 638–645.
[18] Y.A. Litvinov, et al., Observation of non-exponential orbital electron capture decays of hydrogen-like ^{140}Pr and ^{142}Pm ions, Phys. Lett. B 664 (3) (2008) 162–168.
[19] National Nuclear Data Center Brookhaven National Laboratory, ⟨http://www.nndc.bnl/gov/⟩, 1996.
[20] N. Winckler, et al., Orbital electron capture decay of hydrogen- and helium-like ^{142}Pm ions, Phys. Lett. B 679 (1) (2009) 36–40.
[21] H. Weick, ATIMA Website. ⟨https://web-docs.gsi.de/~weick/atima/⟩, 2014.